ISSN: 2688-8645

# Rotor Drop Characteristics of Active Magnetic Bearings under Typical Maneuvering Conditions

Junfei Liao, Xiaohu Wang

School of Mechatronic Engineering, Southwest Petroleum University, Chengdu, Sichuan, 610500, China

## Abstract

**To address the critical safety risks of high-speed rotor drop and subsequent rub-impact following the failure of active magnetic bearings (AMBs) in aero-engines, this paper establishes a nonlinear dynamic model for a flexible AMB rotor-protective bearing system that fully couples maneuvering flight loads. The rotor model is constructed based on the Timoshenko beam theory and the finite element method (FEM). By incorporating the Hunt-Crossley nonlinear contact model and the multidimensional maneuvering additional inertial force field, the transient dynamic equations of the system are solved over the entire process using the Newmark-HHT method. Furthermore, the evolutionary laws of the rotor drop impact characteristics under vertical translational overload, rolling maneuvers, and coupled translational-rotational maneuvers are systematically and quantitatively analyzed.**

## Keywords

**Aero Engines; Active Magnetic Bearings; Protective Bearings; Rotor Drop; Mechanical Loads.**

## 1. Introduction

With core advantages such as contactless friction, lubrication-free operation, high-speed adaptability, and dynamic adjustability, Active Magnetic Bearings (AMBs) have become a key technology for the rotor support systems of new-generation high thrust-to-weight ratio aero-engines. However, constrained by magnetic saturation and control systems, their load-carrying capacity makes them highly susceptible to instability under extreme aeronautical operating conditions. This instability can trigger high-speed rotor drop impacts onto touchdown bearings (TDBs), subsequently inducing severe rub-impact, bearing failure, or even cascading failures, which remains the core safety bottleneck restricting their engineering applications in aviation [1, 2].

Scholars at home and abroad have conducted extensive research on rotor drop dynamics under a fixed base, improving the analysis of drop contact modeling, evolutionary laws, and protection methods [3-5]. Some studies have also investigated the effects of base excitation and maneuvering loads on AMB rotor systems, clarifying the mechanism of external disturbances on rotor contact behaviors [6-9]. However, most existing studies are based on the assumption of a fixed ground base. For aeronautical maneuvering flight scenarios, research on the coupling effects of translational overload, attitude angle maneuvers, and drop rub-impact remains insufficient. The lack of systematic analysis regarding the instability mechanisms and critical boundaries of rotor drops under maneuvering loads makes it difficult to meet the engineering requirements for the ultimate protection design of AMB systems within the full flight envelope.

Therefore, this paper establishes a nonlinear dynamic model for the drop of aeronautical AMB flexible rotors coupled with maneuvering loads. By fully incorporating the maneuvering inertial effects and nonlinear contact models, and numerically solving the strongly nonlinear dynamic

ISSN: 2688-8645

equations of the system, this study analyzes the full-process evolutionary laws and parameter sensitivity of the rotor drop. Furthermore, it reveals the influence mechanisms and instability boundaries of typical maneuvering conditions on the drop characteristics. The research results can provide theoretical support for the safety protection design of AMB systems in aero-engines.

## 2. Dynamic Modeling and Solution Methods for Rotor Drop Systems

### 2.1. Basic Assumptions and Coordinate System Definition

To accurately characterize the multi-body coupling relationship among the aircraft maneuvering flight, casing base motion, and rotor elastic vibration, three sets of orthogonal coordinate systems following the right-hand rule are defined in this paper. These coordinate systems provide a unified kinematic reference for introducing maneuvering loads and modeling system dynamics [10]. The definitions of the coordinate systems are illustrated in Figure 1.

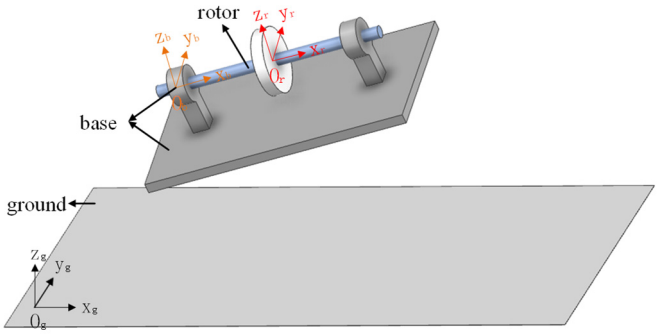


**Figure 1.** Schematic diagram of coordinate system

Specifically, the inertial coordinate system $R_g(O_gx_gy_gz_g)$ is fixed to the Earth's surface. Serving as the basic reference frame for absolute motion, it is used to describe the spatial translation and global attitude transformation of the aircraft. The base coordinate system $R_b(O_bx_by_bz_b)$ is fixed to the aero-engine casing support and performs translational and attitude maneuvers synchronously with the aircraft body. It acts as the core bridge connecting the aircraft maneuvering loads with the rotor system, and its initial axis coincides with the axial direction of the rotor. The rotor coordinate system $R_r(O_rx_ry_rz_r)$ is fixed to the rotor shaft sections and rigid disk units, which is used to describe the bending vibration and rigid body rotation of the rotor relative to the casing base.

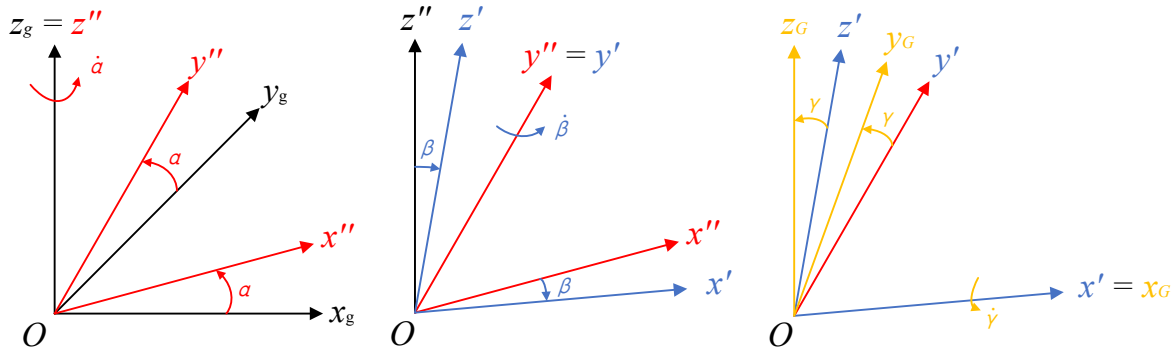


**Figure 2.** Schematic diagram of coordinate system transformation

Adopting the standard Z-Y-X Euler angle transformation method in flight dynamics, this paper derives the total transformation matrix from the inertial coordinate system to the base coordinate system through three successive intrinsic rotations: yaw, pitch, and roll. This

ISSN: 2688-8645

enables the projection transformation of the aircraft's maneuvering attitude angles, angular velocities, angular accelerations, and translational accelerations into the base coordinate system. The angular velocity of the aircraft body relative to the inertial coordinate system is expressed as:

$$\boldsymbol{\omega}_b = \begin{Bmatrix} \omega_{bx} \\ \omega_{by} \\ \omega_{bz} \end{Bmatrix} = \begin{Bmatrix} \dot{f} - \dot{y}\sin q \\ \dot{q}\cos f + \dot{y}\cos q \sin f \\ -\dot{q}\sin f + \dot{y}\cos q \cos f \end{Bmatrix} \tag{1}$$

Further, through the rotational transformation from the base coordinate system to the rotor coordinate system, the transport inertial forces and additional gyroscopic moments induced by maneuvering flight are introduced into the rotor dynamic equations, thereby completing the fully coupled mathematical modeling of the maneuvering loads and the rotor system. The angular velocity of the rotor relative to the inertial coordinate system is expressed as:

$$\omega_r = \omega_{rb} + R_{br}\omega_b = \begin{Bmatrix} \omega_{rbx} \\ \omega_{rby} \\ \omega_{rbz} \end{Bmatrix} + T_x(q_x)T_y(q_y)T_z(q_z) \begin{Bmatrix} \omega_{bx} \\ \omega_{by} \\ \omega_{bz} \end{Bmatrix} \tag{2}$$

## 2.2. Rotor - Protective Bearing Drop Collision Modeling

After the failure of the magnetic bearing, the high-speed rotor will drop onto the protective bearing (touchdown bearing), generating strong nonlinear coupled behaviors of impact and friction. Discarding the traditional rigid support assumption, this paper establishes a double-layer support dynamic model consisting of the rotor, the inner ring of the protective bearing, and the bearing housing. This model accurately characterizes the transmission and dissipation laws of the impact energy, as well as the spin coupling effect of the inner ring during the drop process. The structure of the model is shown in Figure 3.

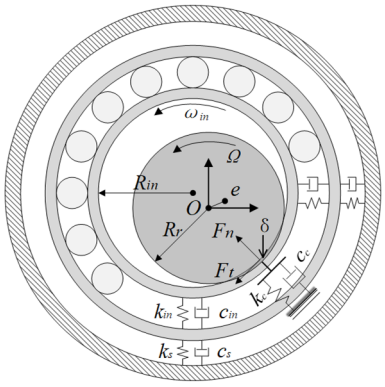


**Figure 3.** Schematic diagram of rotor protection bearing falling and impact

Based on the double-layer support assumption, the model decouples the protective bearing system into two series-connected spring-damper subsystems: the inner ring-rolling element subsystem and the outer ring-housing subsystem. It comprehensively covers the nonlinear contact friction between the rotor and the inner ring, the rotational dynamics of the inner ring, and the stiffness and damping characteristics of both the bearing interior and the housing. In the figure, $\Omega$ denotes the nominal rotational angular velocity of the rotor, $\omega_{in}$ is the instantaneous angular velocity of the inner ring of the protective bearing, $R_r$ is the radius of the rotor journal, $R_{in}$ is the radius of the inner ring raceway, $\delta$ represents the contact deformation. Additionally, $F_n$ and $F_t$ are the normal contact force and tangential friction force at the contact interface, respectively; $k_{in}$ and $c_{in}$ denote the internal equivalent stiffness and damping of the protective bearing, while $k_s$ and $c_s$ are the equivalent stiffness and damping of the bearing housing support.

ISSN: 2688-8645

Assuming the displacement coordinates of the rotor journal center are $q_r = [y_r, z_r]^T$, and the displacement coordinates of the geometric center of the protective bearing inner ring are $q_{in} = [y_{in}, z_{in}]^T$.

The radial displacement of the rotor center at this node is defined as: $r = \sqrt{y_r^2 + z_r^2}$

The radial contact deformation δ between the rotor and the protective bearing can be defined as:

$$d = \begin{cases} \sqrt{(y_r - y_{in})^2 + (z_r - z_{in})^2} - c, & d > 0 \\ 0, & d \le 0 \end{cases} \tag{3}$$

To overcome the limitations of the traditional Hertz contact model, which fails to characterize impact energy dissipation, and the linear viscoelastic model, which exhibits a discontinuity in the initial contact force, this paper adopts the Hunt-Crossley nonlinear viscoelastic contact model [11， 12]. This model can accurately capture the elastic deformation and internal material damping dissipation characteristics during the impact process of metallic contact pairs, while ensuring the continuity of the numerical solution. The expression for the normal contact force is given by:

$$F_n = \begin{cases} K_c \delta^n + b\delta^n \dot{\delta} & , \quad \delta > 0 \\ 0 & , \quad \delta \le 0 \end{cases} \tag{4}$$

Where $K_c$ is the Hertzian contact stiffness coefficient; $n$ is the force exponent, and for the contact between the inner ring of the protective bearing and the rotor, the line contact coefficient $n$ = 10/9 and $q$ = 1 are typically adopted; $\dot{\delta}$ denotes the normal relative impact velocity. For the parameter $b = 3/2\lambda K_c$ , $\lambda$ represents an empirical damping factor directly related to the material's coefficient of restitution, which is primarily used to control the energy dissipation rate during the impact process.

To avoid the numerical singularity of the classical Coulomb friction model at zero relative velocity, a modified Coulomb friction model smoothed by a hyperbolic tangent function is adopted in this paper, which is expressed as:

$$F_t = -\mu F_n \tanh\left(\frac{v_\tau}{v_{tol}}\right) \tag{5}$$

Where $\mu$ is the dynamic friction coefficient of the contact interface; $v_t$ is the tangential relative sliding velocity at the contact point, which is jointly determined by the rotation of the rotor and the inner ring.

To accurately reproduce the strong coupling effect between friction and inner ring spin, the rotational dynamic equation of the protective bearing inner ring is established as follows:

$$J_{in} \frac{d\omega_{in}}{dt} = T_f - T_{res} \tag{6}$$

Where $J_{in}$ is the moment of inertia of the inner ring, $T_f$ is the driving friction torque, and $T_{res}$ is the internal friction torque of the bearing.

Based on the double-layer support assumption, the translational dynamic governing equations of the protective bearing inner ring-outer ring-housing system can be expressed as:

$$M_{\sup}\ddot{q}_{\sup} + C_{\sup}\dot{q}_{\sup} + K_{\sup}q_{\sup} = -F_c \tag{7}$$

Where $M_{sup}$, $C_{sup}$, and $K_{sup}$ are the mass matrix, damping matrix, and stiffness matrix of the protective bearing support system, respectively, which are assembled from the stiffness and damping parameters of the bearing interior and the housing; $q = [y_{sup}, z_{sup}]^T$ is the generalized coordinate vector of the support system, and $F_c$ is the contact force vector between the rotor and the inner ring, containing normal and tangential components.

ISSN: 2688-8645

## 2.3. System Finite Element Modeling and Numerical Solution Method

Using the Timoshenko beam theory and the finite element method (FEM), this paper conducts the discretization modeling of the aero-engine flexible rotor-protective bearing system. The finite element discretized nodes and the topological relations of the system are illustrated in Figure 4.

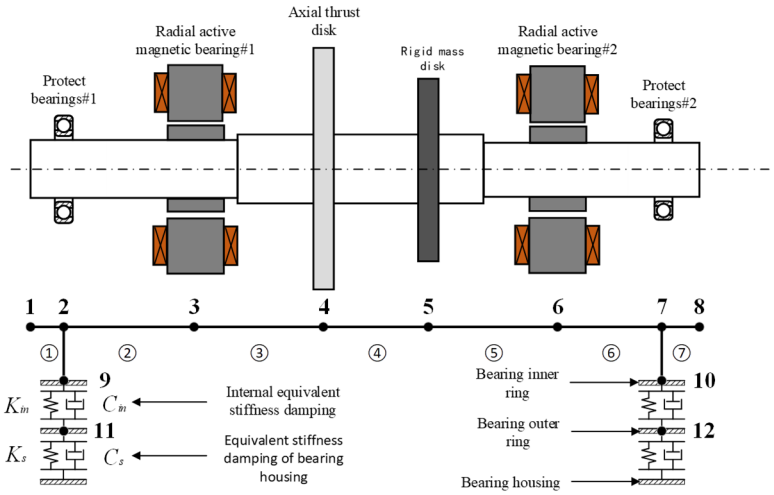


**Figure 4.** Schematic diagram of the system finite element model

During the modeling process, the rotor shaft system is discretized into 7 shaft elements and 8 beam nodes. Each beam node contains a total of 4 degrees of freedom (DOFs): radial translational displacements in the *y* and *z* directions, and rotational angles around the *y* and *z* axes. The left and right protective bearings each contain 2 lumped mass nodes representing the inner and outer rings, with 2 radial translational DOFs considered for each node. The total number of generalized coordinate DOFs for the entire system is 40, among which the rotor system accounts for 32 DOFs and the protective bearing support system accounts for 8 DOFs.

For the discretized rotor system, the models for the rigid disk unit, elastic shaft element, and mass unbalance are constructed respectively. The rigid disk unit comprehensively considers translational inertia, high-speed gyroscopic effects, and maneuvering load coupling terms. For the elastic shaft element, the shape functions are constructed utilizing modified Hermite polynomials, and the mass and stiffness matrices incorporating shear deformation are derived. Concurrently, a mass unbalance excitation force model is established to reproduce the coupling effect of centrifugal forces.

Through the principles of matrix expansion and superposition in FEM, the global assembly of the characteristic matrices for each element is completed, ultimately establishing the whole-system dynamic governing equations for the rotor drop under maneuvering flight conditions:

$$\begin{aligned}&[M]\{\ddot{q}\}+\left(\Omega[G]+\omega_{bx}[C_{bx}]+[C_r]\right)\{\dot{q}\}+\left([K_b]+[K_s]\right)\{q\}\\&+\left(\dot{\omega}_{bx}[K_{\dot{\omega}_{bx}}]+\Omega\omega_{bx}[K_{\Omega\omega_{bx}}]+\omega_{bx}^2[K_{\omega_{bx}^2}]+\omega_{by}^2[K_{\omega_{by}^2}]+\omega_{bz}^2[K_{\omega_{bz}^2}]+\omega_{by}\omega_{bz}[K_{\omega_{by}\omega_{bz}}]\right)\{q\}\\&=F_{base}+F_G+F_{un}+F_c\end{aligned}\tag{8}$$

Where $\{q\}$ is the generalized displacement vector of the rigid disk unit; $\{\dot{q}\}$ is the generalized velocity vector of the rigid disk unit; $\{\ddot{q}\}$ is the generalized acceleration vector of the rigid disk unit; $[M]$ is the mass matrix of the rigid disk unit; $[G]$ is the gyroscopic matrix of the rigid disk unit; $[C_{bx}]$ is the maneuvering parameter damping matrix of the system; $[C_r]$ is the Rayleigh

ISSN: 2688-8645

damping matrix; $[K_b]$ is the bending stiffness matrix of the rotor; $[K_s]$ is the shear stiffness matrix of the rotor; $[K_{\dot{\omega}_{bx}}]$, $[K_{\Omega\omega_{bx}}]$, $[K_{\omega_{bx}^2}]$, $[K_{\omega_{by}^2}]$, $[K_{\omega_{bz}^2}]$, and $[K_{\omega_{by}\omega_{bz}}]$ are the maneuvering parameter stiffness matrices of the system; $\Omega$ is the rotational angular velocity of the rotor; $\dot{\omega}_{bx}$ is the angular acceleration of the base rotating around the $O_x$ axis; $\omega_{bx}$, $\omega_{by}$, and $\omega_{bz}$ are the maneuvering angular velocities of the aircraft body; $F_{base}$ is the maneuvering load induced by maneuvering flight; $F_G$ is the gravity acting on the rigid disk unit; $F_{un}$ is the unbalance force; and $F_c$ is the contact force.

## 3. Calculation Results and Discussion

Based on the established nonlinear dynamic model of the flexible rotor-protective bearing system coupled with maneuvering loads, the Newmark-HHT numerical integration method is employed to solve the system dynamic equations. The integration step size is set to 1e-5 s, and the total simulation duration is 1 s. This fully covers the entire process of rotor drop, rub-impact, and energy dissipation following the failure of the active magnetic bearing (AMB).

**Table 1.** Simulated rotor shaft and disk parameters

| Serial number | 1 | 2 | 3 | 4 | 5 | 6 | 7 | 8 | 9 |
|---|---|---|---|---|---|---|---|---|---|
| Type | Shaft segment unit | | | | | | | Disk unit | |
| Inner diameter (mm) | 0 | | | | | | | 35 | 80 |
| Outer diameter (mm) | 34.5 | 62 | 62 | 62 | 62 | 62 | 39.5 | 210 | 200 |
| Length (mm) | 25 | 48 | 100 | 82 | 80 | 47 | 30 | 14 | 20 |
| Eccentric (mm) | 0 | | | | | | | 0.006 | 0.006 |
| Density (kg/m$^3$) | 7850 | | | | | | | | |

**Table 2.** Parameters for Protective Bearings

| | Protect bearings #1 | Protect bearings #2 |
|---|---|---|
| Outer diameter (mm) | 62 | 68 |
| Inner diameter (mm) | 35 | 40 |
| Shaft diameter (mm) | 34.5 | 39.5 |
| Gap (mm) | 0.25 | 0.25 |
| Width (mm) | 9 | 9 |
| Quality (kg) | 0.107 | 0.125 |

The baseline simulation parameters are adopted from the typical parameters of an aero-engine maglev rotor system (Tables 1 and 2). The baseline operating condition is defined as a fixed base with a g gravitational acceleration. The rated rotational speed of the rotor is 18,000 r/min, the mass eccentricity is 6 μm, and the dynamic friction coefficient of the contact interface is 0.2. For the protective bearing, the internal equivalent stiffness is kin = 1.5 × 108 N/m, and the internal equivalent damping is cin = 300 N·s/m. The equivalent stiffness and damping of the support are ks = 3 × 108 N/m and cs = 2000 N·s/m, respectively. This section systematically analyzes the nonlinear dynamic response laws of the rotor drop under translational overload, attitude rotation, and coupled maneuvering conditions, quantifies the influence mechanisms of

ISSN: 2688-8645

key parameters on the drop impact characteristics, and reveals the instability mechanisms and critical boundaries of the rotor drop under aeronautical maneuvering conditions.

## 3.1. The Effect of Vertical Translational Overload on Rotor Drop

When an aircraft executes maneuvering actions such as pull-up or dive, the translational overload generated along the vertical direction of the airframe is, in its physical essence, a massive static inertial force superimposed on the original gravity field of the system. This additional inertial force field directly reconstructs the spatial potential energy distribution of the rotor, thereby altering the static equilibrium baseline and the available rebound space within the clearance of the protective bearing.

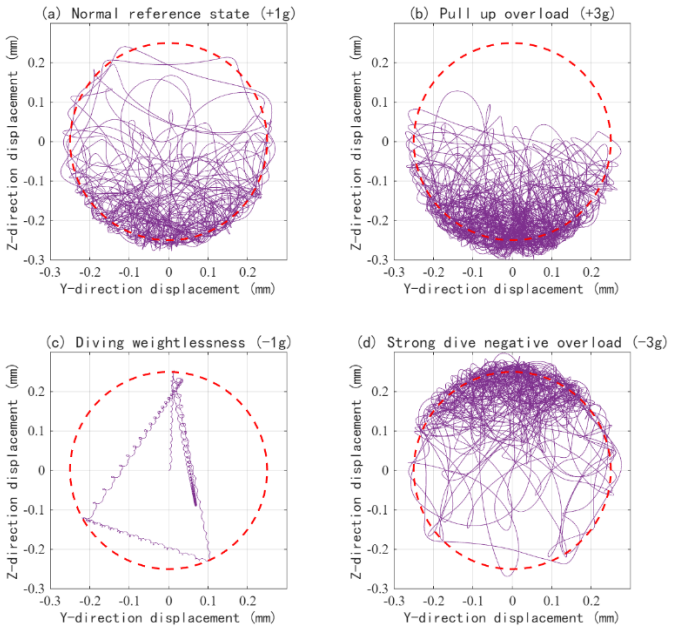


**Figure 5.** Two-dimensional shaft center trajectory under various vertical overload conditions

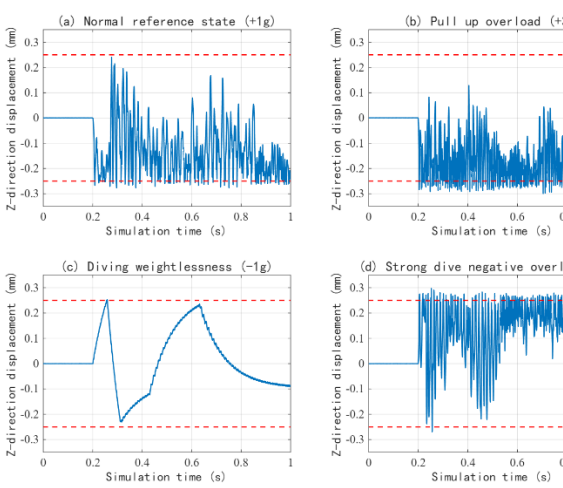


**Figure 6.** Displacement time history diagram

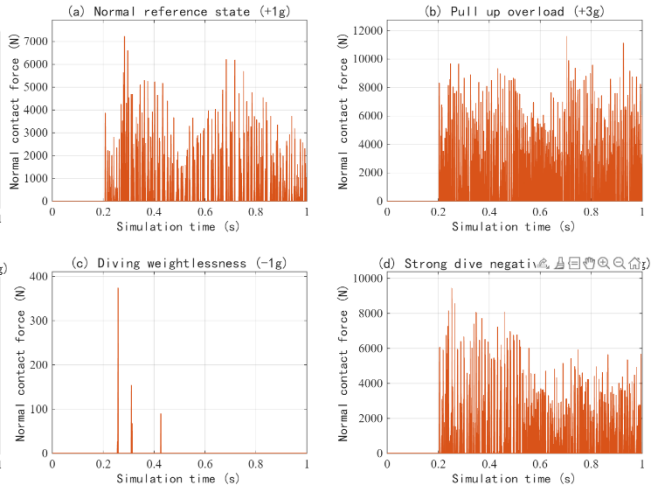


**Figure 7.** Contact Force Time History Diagram

The transient drop response and time-history spectra, as shown in Figures 5, 6, and 7, quantitatively reveal the influence of this mechanism: Under the normal baseline state (+1g), the rotor, dominated by gravity, stabilizes at the bottom of the bearing (at a Z-direction displacement of approximately -0.25 mm) and undergoes local high-frequency reciprocating rub-impact, with the maximum normal contact force of the system reaching approximately

ISSN: 2688-8645

7,000 N. When a pull-up overload (+3g) is applied, a downward static inertial force up to three times that of gravity forcibly presses the rotor against the bottom wall of the bearing, greatly compressing the elastic recovery space of the rotor. The sudden increase in local normal stiffness results in a highly densified distribution of collision points, causing the peak contact force to surge nonlinearly to over 11,000 N. Conversely, under the extreme critical condition of weightlessness during a dive (-1g), the upward maneuvering inertial force cancels out the gravity of the rotor, and the normal constraint of the system approaches zero. The rotor enters a "zero-gravity suspension" wandering state, evolving into a low-frequency, large-scale triangular trajectory within the clearance, with the collision peak dropping sharply to 300–400 N. In contrast, a strong negative dive overload (-3g) forces the dominant force field to reverse, and the massive reverse inertial force drives the rotor to excite severe local full-annular rub-impact in the upper half region.

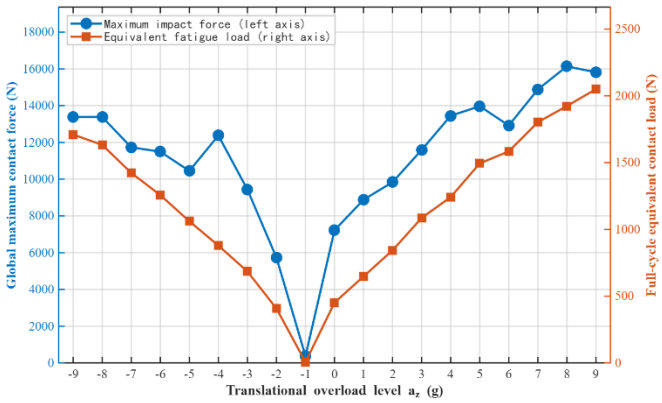


**Figure 8.** Contact force bifurcation diagram under different overload levels.

The bifurcation evolution laws corresponding to the magnitude of translational overload (-9g to +9g), as illustrated in Figure 8, further demonstrate that the drop impact load exhibits a strong "V-shaped" nonlinear characteristic as the overload magnitude increases. The global minimum load point corresponds strictly to the critical point where gravity is completely counteracted (-1g). Furthermore, the damage evolution presents significant asymmetry; the ultimate destructive force induced by a positive overload is generally higher than that of a negative overload of the same magnitude (e.g., the impact force at +9g approaches 16,000 N, while at -9g it is approximately 13,500 N). This is because the positive overload and the Earth's gravity field vector are superimposed in the same direction, maximizing the conversion of transient normal kinetic energy into the elastic strain energy of the contact interface.

Based on the comprehensive analysis above, it can be concluded that the vertical translational overload reconstructs the physical collision boundaries by altering the normal static constraint forces. The extreme compression of the local rebound space is the objective mechanism that induces continuous dense rub-impact and causes the nonlinear amplification of the impact contact force.

## 3.2. Rotor Drop Characteristics under Roll Attitude

The rolling of the casing base around the longitudinal axis not only introduces centrifugal inertial forces and Coriolis forces into the system, but also forms a periodically rotating "equivalent alternating gravity field" within the clearance of the protective bearing. This rotating non-inertial force field completely breaks the energy dissipation equilibrium of the rotor under a single gravity vector, serving as a key excitation source that induces complex nonlinear behaviors of the system.

ISSN: 2688-8645

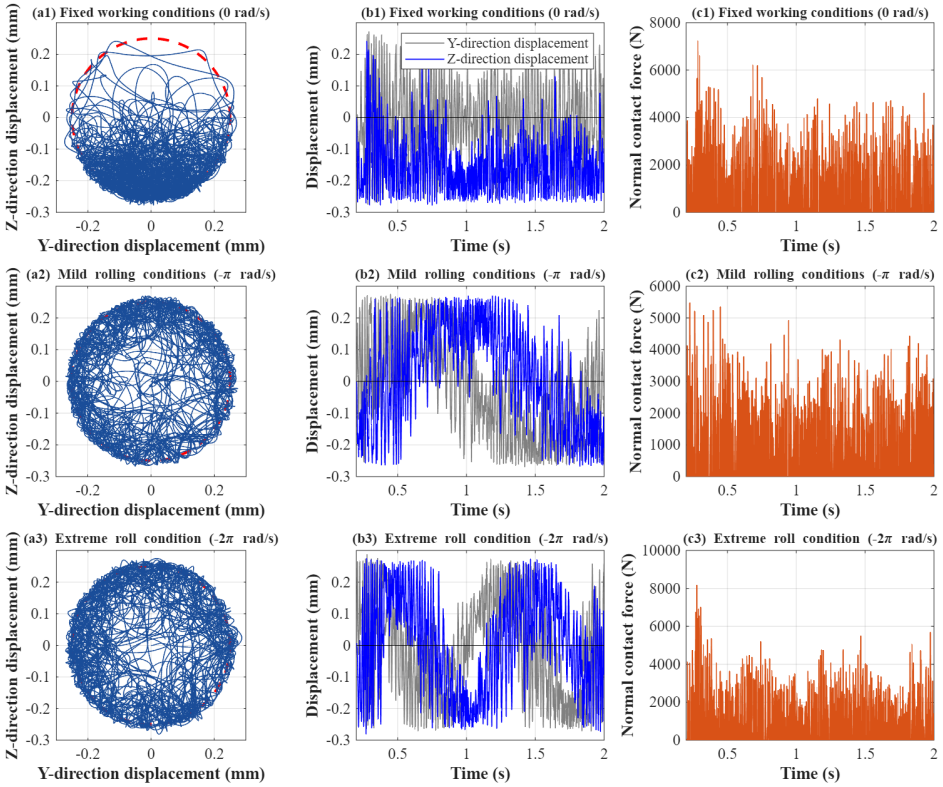


**Figure 9.** Rotor drop response under different roll conditions

The comparison of the responses between the fixed-base and rolling conditions, as shown in Figure 9, clearly demonstrates the evolution of the trajectory topology: under the fixed-base condition (0 rad/s), the rotor maintains stable bottom rub-impact; after introducing a mild rolling (-π rad/s), the centrifugal effect drives the rotor to overcome gravity and perform work, causing the trajectory to deviate and diffuse towards the upper side. When reaching the ultimate rolling (-2π rad/s), the intense alternating inertial force completely breaks through the bottom contact boundary, resulting in the rotor displacement frequently crossing the geometric center. At this time, the shaft orbit evolves into an extremely disordered chaotic state, and the normal contact force deteriorates from local dense pulses to high-frequency, large-amplitude global random oscillations, with the local impact peak approaching 10,000 N.

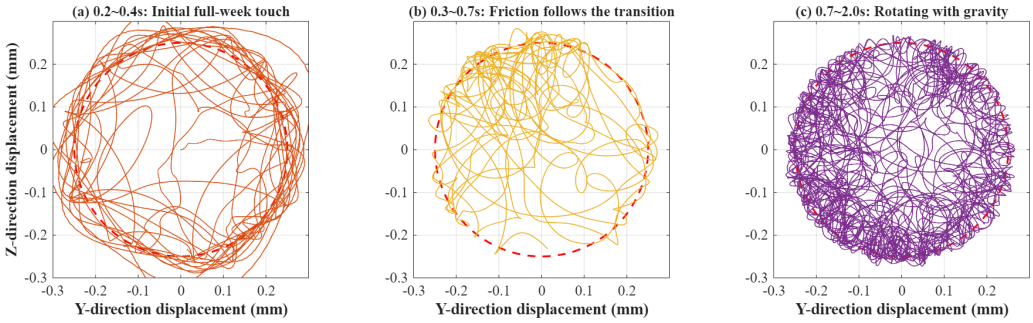


**Figure 10.** Slice diagram of the rubbing trajectory under high-speed extreme rolling condition.

A more profound cross-modal transition law emerges in the extreme condition coupling ultra-high rotational speed (30,000 r/min) and ultimate rolling, as shown in Figure 10. The full cycle of the rotor drop exhibits a typical three-stage dynamic evolution: In the initial stage of the drop, the extremely high relative tangential velocity excites a massive dry friction driving force at the

ISSN: 2688-8645

interface. When the friction driving torque exceeds the system damping, it is highly prone to induce severe backward whirl instability, causing the rotor to tightly cling to the inner wall and produce high-energy full-annular dense collisions. As the kinetic energy of the high-frequency backward whirl is substantially dissipated by sliding friction and inner ring damping, the tangential friction force decays sharply, and the system enters a physical transition period where the friction force loses its dominance and the base's rotational inertial force takes the lead. After the transient friction energy is completely dissipated, the rotor motion is fully taken over by the rolling maneuver. Pulled by the continuously rotating "equivalent gravity field," the rotor clings to the inner wall of the bearing and performs a synchronous circular oscillation at the same frequency as the rolling, with the trajectory stabilizing into a uniform mesh-like circular ring.

Dynamic deduction indicates that the rolling attitude is the core excitation inducing the system to evolve from local rub-impact to global chaotic oscillation. Under the coupling of ultra-high rotational speed, the dynamic interplay between interfacial friction and inertial forces inevitably causes the system to undergo a cross-modal transition from "backward whirl dominated by tangential friction" to "synchronous oscillation pulled by the rotating inertial force field."

## 3.3. Rotor Drop Characteristics under Typical Operating Conditions

As a typical coupled maneuver, horizontal turning requires the casing to bear a lateral centripetal translational overload while inevitably being accompanied by a yaw angular velocity around the spatial vertical axis. This multidimensional superposition of "translational static load" and "rotational dynamic load" is the most severe boundary for evaluating the ultimate load-carrying capacity of the aeronautical magnetic bearing protection system.

Driven by the turning dynamic envelope with a lateral overload of 3g and a yaw angular velocity of 1.0 rad/s, as shown in Figure 11, the global normal contact force of the rotor exhibits continuous high-amplitude fluctuations. In the transient switching regions of "entering the turn" and "leveling off" where the acceleration undergoes step changes, the system is highly prone to excite abnormal load spikes. Meanwhile, in the steady-state turning phase where the parameters remain constant at high levels, the contact force frequently approaches 10,000 N, which greatly accelerates the rolling contact fatigue of the bearing.

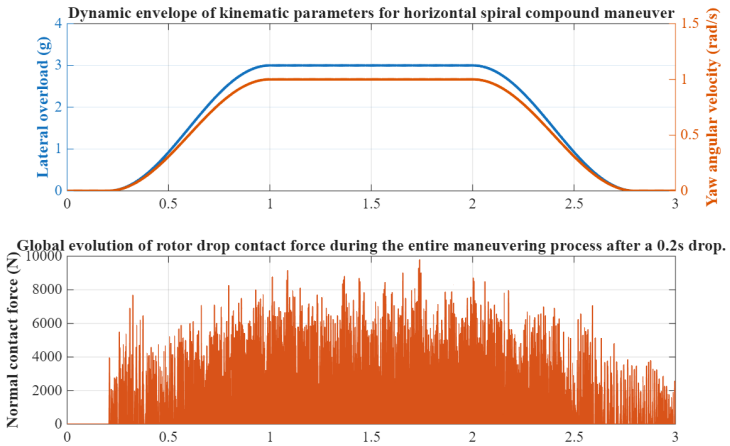


**Figure 11.** Input response during the full dynamic process of hovering.

As shown in Figures 12 and 13, the nonlinear amplification mechanism of the multidimensional coupled loads on the destructive force is confirmed through the comparison of four decoupled conditions: Under the baseline (+1g) condition, the system is loaded symmetrically, and the ultimate impact force on the left and right protective bearings is 7,221 N. When a single lateral

ISSN: 2688-8645

overload (3g) is applied, the lateral static inertial force causes the overall trajectory to deviate laterally and cling to the wall, increasing the peak value to 9,348 N. When a single yaw angular velocity (1.0 rad/s) is applied, the high-speed rotating rotor is excited by the yaw rotation, stimulating a strong additional gyroscopic moment. This moment forces the two ends of the rotor to produce reverse bending deformations, forming an extreme asymmetric eccentric load—the bearing on one side experiences dense overload rub-impact in its lower half, while the other side wanders over a large range, causing the system load to surge to 12,670 N. Under the overload-yaw coupled maneuver, the "lateral displacement bias" and the "gyroscopic asymmetric eccentric load" undergo a nonlinear superposition. The journal on the side with dense rub-impact is pushed to the ultimate clearance by the lateral inertial force; simultaneously bearing the heavy pressure of the gyroscopic moment, it suffers high-frequency extreme crushing, and the ultimate contact impact force is sharply amplified to 16,305 N.

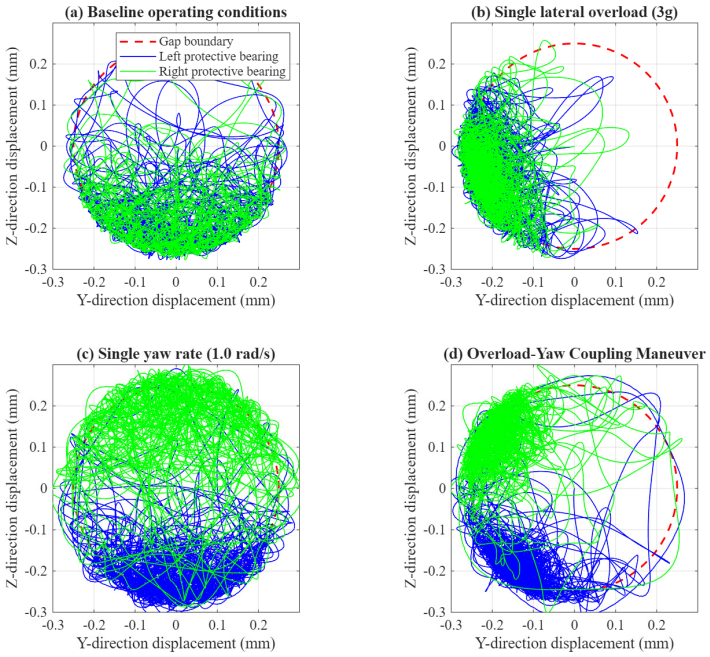


**Figure 12.** Trajectory of the double bearing shaft under different working conditions

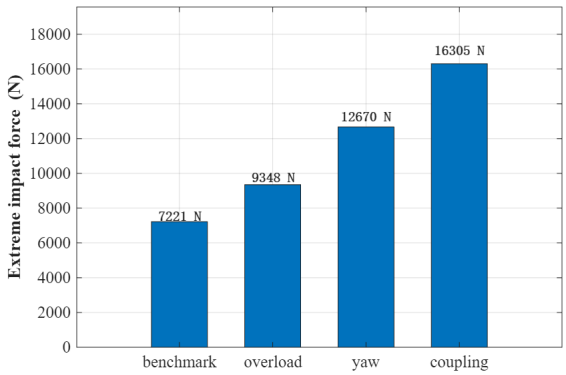


**Figure 13.** Comparison of extreme values of contact force under different working conditions

It can be seen from the above that typical coupled maneuvers have strong nonlinear amplification and asymmetric deterioration effects on the rotor drop damage. The coupling of multidimensional loads not only geometrically compresses the unilateral contact buffer space but also physically severely disrupts the axial load equilibrium of the system through the

ISSN: 2688-8645

gyroscopic effect. This surged unilateral extreme contact eccentric load is the most dangerous mechanical source inducing the local transient collapse of the protection system; therefore, sufficient safety margins against eccentric loading must be reserved in engineering design.

## 4. Summary

Aiming at the critical drop safety risks following the failure of active magnetic bearings (AMBs) in aeronautical maneuvering flight environments, this paper establishes a nonlinear dynamic model for a flexible rotor-protective bearing system that fully couples aircraft translational and attitude maneuvering loads. Through a full-process transient dynamic analysis, the evolutionary mechanisms of multidimensional maneuvering loads on the nonlinear rub-impact behaviors and local impact extremes during the drop are systematically revealed. The main conclusions are drawn as follows:

(1) The vertical translational overload reconstructs the static equilibrium potential energy field of the system, dominating the evolution of the drop collision boundaries. The global maximum contact impact force of the drop exhibits a strong "V-shaped" nonlinear bifurcation characteristic with the increase in overload magnitude, and its global minimum point corresponds strictly to the critical weightless state (-1g) where gravity is completely counteracted. A strong positive overload (e.g., a pull-up maneuver) severely compresses the local rebound recovery space of the rotor, inducing severe continuous dense rub-impact and resulting in a nonlinear surge of the transient impact force.

(2) The "equivalent alternating gravity field" introduced by the rolling attitude maneuver serves as the core excitation source inducing the dropped rotor to evolve towards global chaotic oscillation. Particularly under the coupled boundary of ultra-high rotational speed and ultimate rolling, the dynamic interplay between the interfacial dry friction driving force and the base rotational inertial force compels the rotor system to undergo a typical cross-modal dynamic transition—namely, experiencing a modal shift from the "backward whirl dominated by tangential friction" in the initial drop stage to the "synchronous oscillation pulled by the rotating inertial force field" following energy dissipation.

(3) Typical coupled translational-rotational maneuvers (e.g., horizontal turning) exert strong nonlinear superposition and asymmetric amplification effects on the rotor drop damage. The strong coupling of multidimensional loads not only geometrically compresses the unilateral contact buffer space to an extreme extent but also physically disrupts the axial load equilibrium of the rotor severely through the strong additional gyroscopic effect stimulated by the rotation. The surged unilateral extreme contact eccentric load under the overload-yaw coupling acts as the most dangerous mechanical source directly inducing the local transient collapse of the protection system.

In summary, the influence of aeronautical maneuvering loads on the drop characteristics of the AMB rotor is not a simple linear superposition of individual loads, but exhibits strong spatial coupling and asymmetric deterioration characteristics. The findings of this study extend the safety design criteria for aeronautical magnetic bearing protection systems from the traditional "static baselines" to "dynamic asymmetric multidimensional boundaries." In practical engineering design, sufficient safety margins against eccentric loading must be reserved based on such coupled maneuvering boundaries.

## References

[1] k S. Keogh. Contact dynamic phenomena in rotating machines: Active/passive considerations (Conference Paper)[J]. Mechanical Systems and Signal Processing, 2012, Vol.29: 19-33.

[2] Cao, Jianming , Allaire,et al. Auxiliary bearing system optimization for amb supported rotors based on rotor drop analysis-part i: Rotor drop analysis method[C]//ASME Turbo Expo 2016: Turbomachinery Technical Conference and Exposition. 2016.

[3] Xiao Yu, Jianggui Han and Tingfeng Ming. Dynamic Simulation of a 5 Degrees of Freedom Rotor Dropping on a Protective Bearing[J]. Applied Sciences,2024,Vol.14(7): 2837.

[4] Xiaoxu Pang,Dingkang Zhu,Ming Qiu,et al. Eccentric Rotor Drop Dynamics Study of Vertical Maglev Bearing System[J]. Lubricants,2023, Vol.11(6): 246.

[5] Yili, Z., Yongchun, et al. Dynamic responses of rotor drops onto auxiliary bearing with the support of metal rubber ring(Article)[J]. Open Mechanical Engineering Journal,2015,Vol.9(1): 1057-1061.

[6] Jarroux, Clément,Dufour,et al. Touchdown bearing models for rotor-AMB systems(Article)[J]. Journal of Sound and Vibration,2019, Vol.440(1): 51-69.

[7] Zhu, C.-S. Email Author, Chen,et al. Vibration characteristics of aeroengine's rotor system during maneuvering flight(Article)[J]. Hangkong Xuebao/Acta Aeronautica et Astronautica Sinica,2006, Vol.27 (5): 835-841.

[8] Zhu Chang-sheng,Chen Yong-jun. General dynamic model of aeroengine's rotor system during maneuvering flight[J]. Journal of Aerospace Power,2009, Vol.24(2): 371-377.

[9] Benchun Yao,Zhen Tian,Xu Zhan,et al. Study on Rotor-Bearing System Vibration of Downhole Turbine Generator under Drill-String Excitation[J]. Energies,2024, Vol.17(5): 1176.

[10] Jarroux, Clé,ment,et al. Investigations on the dynamic behaviour of an on-board rotor-AMB system with touchdown bearing contacts: modelling and experimentation. [J]. Mechanical Systems & Signal Processing, 2021, Vol.159: 107787.

[11] MacHado, M., Moreira, et al. Compliant contact force models in multibody dynamics: Evolution of the Hertz contact theory (Article)[J]. Mechanism and Machine Theory,2012, Vol. 53: 99-121.

[12] K. H. Hunt, F. R. E. Crossley. Coefficient of Restitution Interpreted as Damping in Vibroimpact[J]. Journal of Applied Mechanics,1975, Vol.42(2): 440-445.